Gas-Phase Reactivity of Ni^+ with Glycine

L. Rodriguez-Santiago,[†] M. Sodupe,[‡] and J. Tortajada*,[†]

Laboratoire Analyse et Environnement, CNRS UMR 8587, Université d'Evry-Val-d'Essonne, Boulevard Françoise Mitterrand 91025 Evry Cedex, and Departament de Quimica, Universitat Autonoma de Barcelona, Bellaterra 08193 Barcelona

Received: December 11, 2000; In Final Form: March 14, 2001

The reactions between Ni^+ and glycine in the gas phase have been investigated both by means of mass spectrometry and B3LYP density functional calculations. The [Ni−glycine]$^+$ adduct is formed in the ion source. The structure of several coordination modes of Ni^+ to glycine have been determined at the B3LYP level. Calculations have shown that the ground-state structure is a bidentate η^2**-N,O** one in which the Ni^+ cation interacts with the nitrogen atom and the carbonyl oxygen. The MIKE spectrum of the [Ni−glycine]$^+$ ion has also been analyzed and shows that the most important fragmentation corresponds to the loss of water. Other fragmentations are observed to a minor extent, namely loss of CO or loss of CH_2O_2. The possible mechanisms leading to these fragmentations have been studied at the B3LYP level. Among all of the mechanisms studied, the most favorable one starts with the insertion of the Ni^+ metal cation into the C−C bond of the most stable η^2**-N,O** structure.

Introduction

The study of the interaction of transition metal cations with organic and bioorganic compounds in gas phase has been the subject of considerable attention during the past years[1−3] due to the importance of such systems in several fields. For example, transition metal cation complexation of neutral molecules can induce important activation effects, which, under mass spectrometry experiments, lead to specific fragmentations that can provide structural information of the neutral molecules. In particular, in recent years, transition metal cationization has proven to be a very useful tool for the elucidation of the primary structures of proteins.[4−6] The amino acid sequence of peptides can be obtained analyzing the fragmentations induced by transition metal cationization in peptides.

On the other hand, complexes of transition metal cations and different biomolecules play an essential role in many biological processes. In particular, interaction of transition metals and amino acid residues takes place in several processes such as dioxygen transport or electron transfer.[7] In this context, the study of the interaction of transition metals and amino acids, which are the constituents of the peptides, is a topic of high interest.

The gas-phase study of the metal cation-biomolecule complexes helps us to understand their intrinsic properties such as the local interactions that take place between the metal cation and the biomolecule, without the presence of the solvent or counterions. The study of these intrinsic interactions and properties by combining both mass spectrometry experiments and ab initio theoretical methods can provide us a deeper insight into the knowledge of the biological processes that involve metal cations.

Theoretical methods allow us to know the cationization site and the structure of each fragment observed in mass spectrometry experiments. In addition, the theoretical calculations can provide the accurate determination of some relevant magnitudes, such as enthalpies or complexation energies. Finally, by means of computational methods we can elucidate the reaction paths that lead to the observed fragmentations. This combined theoretical and experimental approach has been applied successfully in the past few years in our research group to other metal cationized systems involving small bases of biochemical significance.[8−10]

Glycine is the simplest amino acid and a suitable model to investigate its interaction with transition metal cations, both from experimental and theoretical points of view.

The interaction of different metal cations with glycine and other amino acids has been studied by several authors from an experimental point of view.[11−19] Harrison and co-workers have studied the fragmentation reactions of several Cu^+ and Ni^+ cationized amino acids prepared by fast atom bombardment (FAB).[13,14] The major fragmentations observed involved the elimination of CO, H_2O, and CH_2O_2 in different proportions, depending on the amino acid and the metal cation studied. Hoppilliard and co-workers have reported studies of the formation and fragmentation of the complexes of Ni^+, Cu^+, Co^+ and $FeCl^+$ with several amino acids in plasma desorption mass spectrometry (PDMS).[15,16] In particular, they have studied the fragmentation of the [Ni−glycine]$^+$ system. In their PDMS experiments, the base peak of the spectra corresponds to the imonium ion ($m/z = 30$) whereas the most abundant organometallic fragment corresponds to the loss of CH_2O_2. Lei and Amster have studied the reactions of Fe^+ and Cu^+ with the 20 common amino acids by means of laser desorption/chemical ionization Fourier transform mass spectrometry.[19]

Previous theoretical studies have analyzed the structure of glycine cationized with alkali metal cations[20,23] and copper cations (Cu^+ and Cu^{2+}).[21,22,23] However, to our knowledge, the fragmentation of metal cationized amino acids has not been studied theoretically. Moreover, nobody has consider the interaction of Ni^+ with amino acids from a theoretical point of view. The Ni^+ cation is an open shell system with a d^9 (^2D) ground state. This fact makes the theoretical studies more complex than for other closed shell cations such as Cu^+ or Zn^{2+}.

[†] Laboratoire Analyse et Environnement.
[‡] Universitat Autonoma de Barcelona.

10.1021/jp004461i CCC: $20.00
Published on Web 05/10/2001

For these reasons, we have considered of interest the study of the gas-phase chemistry of the $[Ni-glycine]^+$ system.

In this paper we first study the unimolecular decomposition process of $[Ni\text{-}glycine]^+$ by means of mass-analyzed ionic kinetic energy spectroscopy (MIKES). The $[Ni-glycine]^+$ ion is obtained first in a fast atom bombardment (FAB) ion source. The recorded spectra show that $[Ni-glycine]^+$ undergoes fragmentation by several distinct pathways, the most important peak corresponding to the loss of a H_2O molecule.

The complete interpretation of the reactivity requires a reliable description of the potential energy surface (PES) of the system in terms of local minima and transition states connecting them. Thus, we have studied theoretically the possible modes of coordination of Ni^+ to glycine along with the possible pathways of the decomposition that lead to the experimentally observed fragments. Energies, geometries, and vibrational frequencies of the different investigated species have been determined using the B3LYP density functional method.

Experimental Section

The mass spectrometric measurements were recorded on a double-focusing ZAB−HSQ mass spectrometer (Fisons Instruments) of BEqQ configuration[24] (B and E represent the magnetic and electric sectors, q is a collision cell consisting of a rf-only quadrupole, and Q is a mass selective quadrupole). This mass spectrometer is equipped with a FAB ion source using the following conditions: accelerating voltage 8 kV, neutral xenon beam of 7 keV, and neutral current of ∼10 A. Glycine was dissolved in a thioglycerol matrix to which a few drops of a saturated aqueous $NiSO_4$ solution were added. A few microliters of the resulting mixtures were transferred onto the FAB probe tip.

The unimolecular reactions of the mass selected organometallic ions, corresponding to $[glycine-Ni^+]$ metastable ions, which take place in the second field-free region (second FFR) behind the magnet, were studied by mass-analyzed ion kinetic energy (MIKE) spectroscopy. This technique consists of focusing the relevant ion magnetically into the second FFR and detecting the products of spontaneous fragmentations by scanning the electrostatic analyzer, E. The MIKE spectra were recorded at a resolving power of ∼1000.

Computational Details

Full geometry optimizations and harmonic vibrational frequency calculations of the different species under consideration have been performed using the nonlocal three parameter hybrid exchange B3LYP density functional method.[25] To identify the minima connected by a given transition state, we have carried out intrinsic reaction coordinate (IRC) calculations at the same level of theory. The B3LYP method has proven to provide accurate results for many transition-metal-containing systems.[26−30] In particular, the adequacy of this method for the study of different metal cation−ligand systems has been shown in several papers.[9,10,21,22,31] For several small compounds, the B3LYP method has been shown to provide metal cation affinities that are in good agreement with experimental data.[23,31,32] Recently, Luna and co-workers[32] have studied a wide set of small systems using CCSD(T), B3LYP and G2-based methods. They have found the G2 and the G2(MP2) methods to fail dramatically when trying to reproduce Cu^+ binding energies. However, the B3LYP method yields Cu^+ binding energies in fairly good agreement with the experimental values. Moreover, a previous study on similar metal cation−glycine systems[33] has shown that the B3LYP energy barriers reproduce reasonably well the CCSD(T) results. On the other hand, recent studies on the conformational behavior of glycine and other amino acids[34−37] have shown that the B3LYP method provides structural parameters that are very similar compared with MP2 and vibrational frequencies and intensities that are in excellent agreement with the experimental data.

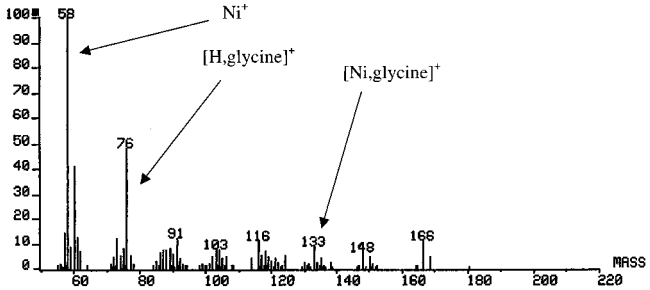

Figure 1. FAB spectrum of glycine dissolved in a matrix of thioglycerol containing $NiSO_4$.

Geometry optimizations and frequency calculations have been performed using the following basis set. The Ni basis set is a [8s 4p 3d] contraction of the (14s 9p 5d) primitive set of Wachters[38] supplemented with two diffuse p and one diffuse d function.[39] The final basis set is of the form (14s 11p 6d)/[8s 6p 4d]. The C, N, and O basis set is the (9s 5p)/[4s 2p] set developed by Dunning,[40] supplemented with a valence diffuse function ($\alpha_{sp} = 0.0438$ for carbon, $\alpha_{sp} = 0.0639$ for nitrogen, and $\alpha_{sp} = 0.0845$ for oxygen) and one d polarization function ($\alpha = 0.75$ for carbon, $\alpha = 0.80$ for nitrogen, and $\alpha = 0.85$ for oxygen). For H, the basis set is the (4s)/[2s] set of Dunning,[40] supplemented with a valence diffuse function ($\alpha_{sp} = 0.036$) and a p polarization function. This basis set is referred to as D95++-(d, p) in the Gaussian 98 program.[41] Hereafter, this basis set will be referred as Basis 1.

Single-point calculations at the B3LYP level have been carried out using a larger basis set. The Ni basis set is augmented by a single contracted set of f polarization functions based on a three-term fit to a Slater type orbital,[42] which leads to a (14s 11p 6d 3f)/[8s 6p 4d 1f] basis set. This enlarged basis set for the metal is combined with the 6-311+G(2df, 2p) set[43] for the rest of the atoms. This enlarged basis set will be denoted as Basis 2.

To analyze the nature of the bonding, natural bond orbital (NBO) analysis of Weinhold and Carpenter has been used.[44] All B3LYP reported calculations have been carried out with the Gaussian 98 program.[41]

Results and Discussion

Unimolecular Reactivity of the $[Ni-Glycine]^+$ Ion. Fast atom bombardment of glycine dissolved in a matrix of thioglycerol containing $NiSO_4$ produces abundant $[Ni-glycine]^+$ adduct at $m/z = 133$. It is worth noting that although the oxidation state of the Ni atom in the salt was +2, only Ni^+ adducts were obtained under FAB conditions. This implies the reduction of the metal cation from Ni^{2+} to Ni^+. This has been reported previously by other authors.[45] Besides $[Ni-glycine]^+$, the mass spectrum shown in Figure 1 indicates that other species such as protonated glycine at $m/z = 76$ are observed.

The unimolecular decomposition of the $[Ni-glycine]^+$ adduct has been investigated, and the MIKE spectrum is shown in Figure 2. The spectrum shows different fragmentations of the $[Ni-glycine]^+$ ion. The major fragmentation corresponds to its dissociation to produce an $[Ni-C_2NOH_3]^+$ ion resulting from the elimination of H_2O at $m/z = 115$. This is the base peak of

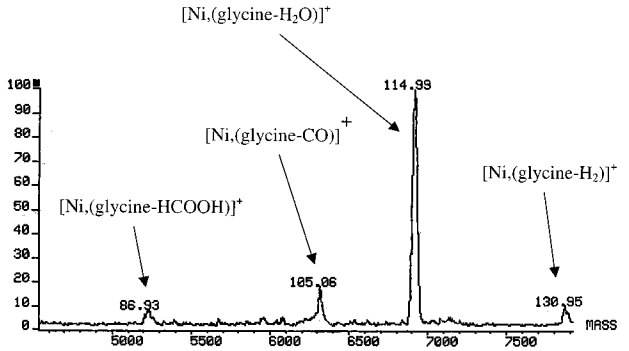

Figure 2. MIKE spectrum of the [Ni−glycine]$^+$ complex at *m*/*z* 133.

the MIKE spectrum. Besides this fragmentation, the [Ni−glycine]$^+$ ion shows other remarkable losses, namely that of CO at $m/z = 105$ (17%) and CH_2O_2 at $m/z = 87$ (7%).

To clarify which hydrogen atoms are involved in the loss of water, the same mass spectrum analysis has been done using deuterated glycine [NH_2-CD_2-COOH]. The obtained MIKE spectrum is very similar to that obtained previously. Again, the base peak of the spectrum, at $m/z = 117$, corresponds to the elimination of H_2O, thus indicating that the hydrogen atoms involved in this fragmentation are those of the OH and NH_2 groups. The same trend is observed in the elimination of CH_2O_2 at $m/z = 89$ (6%).

To rationalize these experimental findings we have studied, by means of the B3LYP method, the most important features of the [Ni−glycine]$^+$ potential energy surface. First, we have considered the possible coordination modes of Ni^+ to glycine. Second, we have explored the stationary points of the possible mechanisms leading to the experimentally observed fragments.

Coordination Modes of the [Ni−Glycine]$^+$ Complex. The relative stability of the different conformational isomers of glycine has been studied extensively. The starting structures involve coordination of Ni^+ on the different electron-rich sites of glycine while retaining hydrogen bonding in glycine as much as possible (as intramolecular hydrogen bonds are responsible for the stability of amino acids). The zwitterionic structure of glycine is not a minimum on the potential energy surface; however, the strong ionic interaction between Ni^+ and the negatively charged end of the zwitterion could stabilize this form. Because of that, we have also considered the coordination of Ni^+ to zwitterionic glycine. Most of these structures have already been considered in previous studies on cationized glycine.[20,21,22]

Figure 3 shows the obtained minima for the [Ni−glycine]$^+$ adduct. Among all of the possibilities considered, only these structures have been characterized as minima. The computed relative energies of the different isomers are shown in Table 1. It can be observed in Figure 3 that five structures have C_s symmetry and four structures have C_1 symmetry. For all of these C_1 symmetry cases, the corresponding C_s structure has been computed to be a transition state connecting two equivalent C_1 isomers. In all cases the distortion of the C_1 structures with respect to the corresponding C_s structures is small, the energy difference being smaller than 0.2 kcal/mol at the B3LYP/Basis 1 level.

The most stable structure, ***η*^{2}-N,O (1)**, corresponds to the metal cation interacting with the nitrogen atom and with the carbonyl oxygen. This structure is almost planar and implies the formation of a five-membered ring. The same structure was found to be the most stable in the case of Cu^+,[21,22] and in the case of the alkali cations Li^+ and Na^+.[20] The second most stable

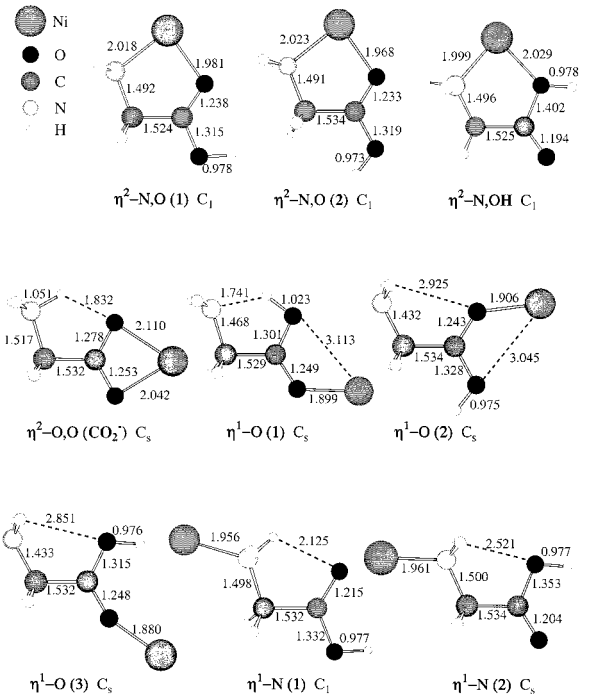

Figure 3. B3LYP optimized geometries for the different minima of the [Ni−glycine]$^+$ complex. Distances are in Å, and angles are in degrees.

TABLE 1: Relative Energies of the Different Structures of the [Ni−Glycine]$^+$ Complex (in kcal/mol)

structure	B3LYP/basis 1	B3LYP/basis 2
η^2-N,O (1)	0.0	0.0
η^2-N,O (2)	6.5	5.8
η^2-N,OH	12.4	12.6
η^2-O,O (CO_2^-)	13.9	14.2
η^1-O (1)	18.0	18.3
η^1-O (2)	30.6	29.2
η^1-O (3)	33.9	33.0
η^1-N (1)	21.5	21.3
η^1-N (2)	24.8	25.0

structure, ***η*^{2}-N,O (2)**, corresponds to the same coordination but with a trans carboxylic group instead of cis. The energy difference of these two structures is in agreement with the energy difference between similar structures involving a cis or a trans carboxylic group, for example in the most stable conformer of glycine where the difference is 5.6 kcal/mol at the B3LYP/D95++(d, p) level. This structure lies 6.5 kcal/mol above the most stable one. The ***η*^{2}-N,OH** and ***η*^{2}-O,O(CO_2-)** structures lie very close in energy (12.4 and 13.9 kcal/mol above the ground-state structure respectively, at the B3LYP/Basis 1 level) and correspond to the Ni^+ interacting with the nitrogen atom and the hydroxyl oxygen (structure ***η*^{2}-N,OH**) and to the Ni^+ interacting with both oxygens of zwitterionic glycine (structure ***η*-O,O(CO_2-)**). The remaining five structures lie higher in energy (more than 18 kcal/mol) above the most stable one, including structure ***η*^{1}-O (1)** (18.0 kcal/mol), which was found to be approximately of the same energy as ***η*^{2}-N,OH** and ***η*^{1}-O (CO_2-)** in the case of [Cu−glycine]$^+$. This structure corresponds to the interaction of Ni^+ with the COOH group of neutral glycine.

Several factors can determine the relative energy of these structures, the main ones being the electrostatic interaction, the metal−ligand repulsion, the charge transfer, the polarization of glycine due to the metal cation and the relative energy of the glycine conformer in the complex with regard to the most stable

TABLE 2: Natural Population Analysis: Net Atomic Charge and Spin Density of Ni

structure	charge	spin
η^2-N,O (1)	.82	.92
η^2-N,O (2)	.83	.92
η^2-N,OH	.83	.92
η^2-O,O (CO_2^-)	.84	.93
η^1-O (1)	.89	.97
η^1-O (2)	.90	.97
η^1-O (3)	.92	.97
η^1-N (1)	.85	.97
η^1-N (2)	.85	.97

TABLE 3: Different Contributions to the Total Interaction Energy of (+)−glycine (see text).

structure	E_{dif}	E_{elec}	E_{pol}	$E = E_{dif} + E_{elec} + E_{pol}$	ΔE^a
η^2-N,O (1)	7.8	−60.5	−33.8	−86.5	0.0
η^2-N,O (2)	14.4	−60.5	−33.6	−79.7	6.8
η^2-N,OH	7.0	−49.4	−32.7	−75.1	11.4
η^2-O,O (CO_2^-)	24.9	−67.5	−27.6	−70.2	16.3
η^1-O (1)	3.1	−47.0	−23.2	−67.1	19.4

[a] ΔE are relative energies (in kcal/mol).

structure of glycine. To gain further insight into some of these factors, the binding energy of glycine to a point charge has been computed for each coordination in three steps. First, we have computed the energy difference between the glycine unit in the complex and glycine in its ground-state structure (E_{dif}). Second, we have computed the energy lowering of the deformed glycine in the presence of a single point charge without allowing electronic relaxation, that is, the electrostatic interaction (E_{elec}). The point charge is placed at the metal−ligand distance. Finally, we have allowed the electronic relaxation of glycine, to obtain the polarization term (E_{pol}). Using this point charge model, Bertran et al.[22] have shown that the energy ordering of the different conformers in $[Cu-glycine]^+$ can be understood in terms of the these three contributions, the charge transfer being almost constant in all cases. Moreover, they pointed out that the observed deviations in the relative energies of the different isomers between the $[Cu-glycine]^+$ and the point-charge−glycine systems were probably due to small changes in metal−ligand repulsion.

The Ni^+ net charges shown in Table 2 indicates that charge transfer is almost constant for all the isomers, as found in the case of $[Cu-glycine]^+$. Table 3 shows the different contributions to the binding energy of glycine to a point charge for the five most stable coordinations. As expected, the polarization term is larger for the structures where the point charge interacts with the amino group, due to the larger polarizability of the nitrogen atom, and the largest electrostatic term corresponds to the zwiterionic structure. It can be observed that the computed relative energies using a point charge reproduce quite well the relative energies of the $[Ni-glycine]^+$ system. It should be noted that the deviations are smaller than in the case of $[Cu-glycine]^+$, indicating that the variation in metal−ligand repulsion between the different structures is smaller in $[Ni-glycine]^+$ than in $[Cu-glycine]^+$. For these reasons, we can conclude that the differences in the relative energies of $[Ni-glycine]^+$ can be explained in terms of the electrostatic and polarization energies and the relative stability of the glycine conformer involved in the complex with respect to the most stable structure of glycine.

The main difference between Cu^+ and Ni^+ is found in the ***η*²-O,O(CO_2^-)** structure. That is, while for $[Cu-glycine]^+$ the two Cu^+-O distances are very different (2.943 and 1.897 Å), for the Ni^+ complex the two Ni^+-O distances are much more similar (2.110 and 2.042 Å), in such a way that glycine acts as a bidentate ligand. All attempts to locate a monodentate structure in the $[Ni-glycine]^+$ have led to the bidentate one. This behavior of $[Cu-glycine]^+$ was attributed to the fact that Cu^+, which has a d^{10} ground-state electronic configuration, prefers an unsymmetrical interaction in order to minimize repulsion between its occupied d shell and the lone pairs of oxygens. Ni^+ has a d^9 configuration, and the ground electronic state of $[Ni-glycine]^+$ is a $^2A'$ state, the open shell lying on the symmetry plane. Thus, metal−ligand repulsion is smaller for Ni^+ than for Cu^+ and so, in the case of $[Ni-glycine]^+$, the electrostatic interaction between the metal cation and the oxygens of the COO^- group in the zwitterionic structure compensates the metal−ligand repulsion, favoring the symmetrical position of the Ni^+ cation.

SCHEME 1

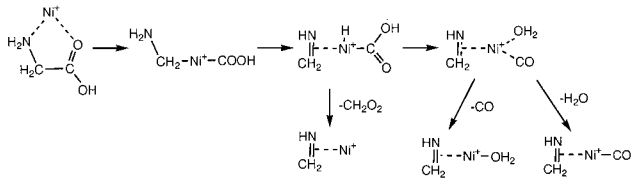

The remaining structures lie higher in energy and were not considered in the study of $[Cu-glycine]^+$. Structures ***η*¹-O (2)** and ***η*¹-O (3)** correspond to the interaction of Ni^+ with the COOH group of neutral glycine. However, these cases differ from structure ***η*¹-O (1)** in the sense that in ***η*¹-O (2)** and ***η*¹-O (3)** there is no intramolecular hydrogen bond in the glycine unit. Structures ***η*¹-N (1)** and ***η*¹-N (2)** correspond to the metal interacting with the nitrogen of two different isomers of neutral glycine.

It can be observed in Table 1 that the use of a larger basis set does not produce important changes in the computed relative energies of the different structures.

The calculated Ni^+-glycine binding energy, 84.6 kcal/mol at the B3LYP/Basis 1 level and 83.2 kcal/mol at the B3LYP/Basis 2 level, is somewhat larger than the binding energy computed for Cu^+-glycine, 75.2 kcal/mol at the B3LYP/Basis 1 level. This is not surprising considering that the metal−ligand distances are smaller in $[Ni-glycine]^+$, due to the smaller metal−ligand repulsion and thus, the electrostatic interaction is larger.

Reactivity of $[Ni-Glycine]^+$ Adducts. As shown previously, the major fragmentation observed in the MIKE spectrum corresponds to the loss of H_2O. Other fragmentations, observed in a much smaller proportion, correspond to the loss of CO, CH_2O_2, and H_2. In the present work, we have not focused our attention into the H_2 fragmentation. The MIKE spectrum obtained using deuterated glycine shows that the hydrogen atoms involved in the fragmentations come from the amino and hydroxyl groups. Thus, to obtain the fragmentation of a water molecule, a hydrogen atom has to be transferred from the amino group to the hydroxyl group of glycine. This reduces the number of possible mechanisms involved in the observed fragmentations.

First of all, the reaction can start with the insertion of the Ni^+ metal cation into the C−C bond of the most stable ***η*²-N,O (1)** structure, as proposed previously by several authors[12−16] for other metal cationized amino acid systems. This possible mechanism is shown in Scheme 1. After the C−C insertion of the metal atom, a hydrogen atom can migrate from the NH_2 group to the OH group through Ni^+-H formation, leading to a complex that can be a precursor for the loss of H_2O or/and CO.

The second possible pathway can start with the insertion of the metal atom into the C−OH bond of the ***η*²-N,OH** structure

SCHEME 2

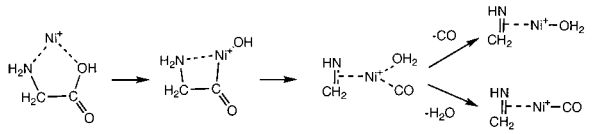

SCHEME 3

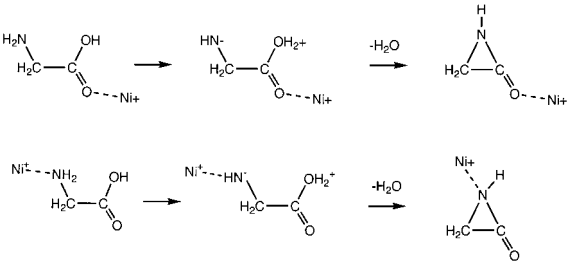

as shown in Scheme 2. After Ni^+ insertion, this path can lead to the same complex as the previous one. The third possibility involves noninsertion mechanisms. A hydrogen atom can be transferred from the NH_2 group to the hydroxyl group in the η^1**-O (3)** and η^1**-N (2)** structures, as shown in Scheme 3. The complexes obtained after the hydrogen transfer can dissociate into $H_2O + [Ni^+{-}OCCH_2NH]$.

To gain some insight into the possible mechanisms associated with the observed fragmentations, we have explored the corresponding potential energy surface (PES) by means of the density functional B3LYP method. In all of the reported calculations, the energy corresponding to the ground state reactants $Ni^+ +$ glycine has been taken as reference.

C−C Insertion Mechanism. Figure 4 shows the obtained mechanism which originates from the insertion of the metal cation into the C−C bond of the most stable η^2**-N,O (1)** structure. It can be observed that all of the computed transition states and final dissociation products lie below the reactants. The transition state **TS1** connects the η^2**-N,O (1)** structure with the Ni inserted species **CC1**, which is 40.7 kcal/mol above the η^2**-N,O (1)** structure. This species can easily evolve through a Ni−C rotation to the **CC2** structure. It should be noticed that the Ni^+ insertion into the C−C bond of the η^2**-N,OH** structure yields the same **CC2** isomer. Thus, the η^2**-NOH** structure can also be a precursor in this mechanism.

Starting from isomer **CC2**, two distinct pathways are possible. The first one, **I**, corresponds to a direct transfer of a hydrogen atom from NH_2 to the carbon atom of the COOH group, leading to a very stable complex (−82.5 kcal/mol) noted as **CC4** in Figure 4. This step takes place through a transition state, **TS2**, which is only 1.4 kcal/mol lower in energy than the reactants. The **CC4** isomer is a dicoordinated complex and can dissociate to produce $Ni^+{-}CHNH_2 + HCOOH$ without barrier in excess. To confirm this fact, the Ni···O distance was scanned from its value in the equilibrium conformation of **CC2** to a sufficiently long distance. This calculation confirms that no barrier in excess exist for such a dissociation.

The second possibility, **II**, involves a hydrogen transfer from the NH_2 of **CC2** to the hydroxyl oxygen. All attempts to locate a transition state for a direct transfer have failed: all of the tested structures have collapsed either to the transition state **TS2** or to the **CC4** minimum. Moreover, any minimum with the hydrogen attached to the Ni atom, as proposed in Scheme 1, has been found. Thus the migration of the hydrogen atom involves a pathway with several steps. First of all, **CC2** evolves to **CC3** through a barrier of 8.5 kcal/mol. It can be observed in

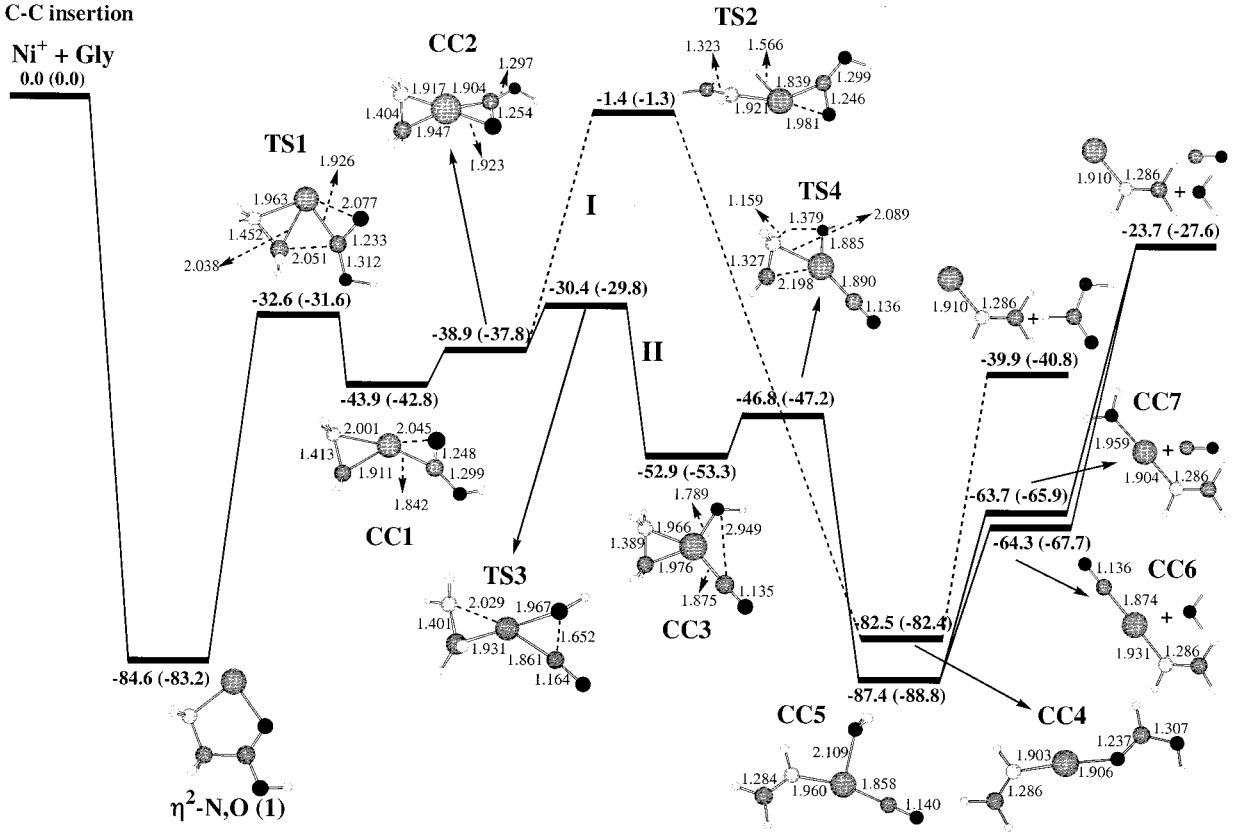

Figure 4. Schematic representation of the potential energy surface associated with the unimolecular reactions of [Ni−glycine]$^+$ starting with the Ni^+ insertion in the C−C bond of the η^2**-N,O(1)** structure. Relative energies are in kcal/mol. Energies computed at the B3LYP/Basis2 level are shown in parentheses.

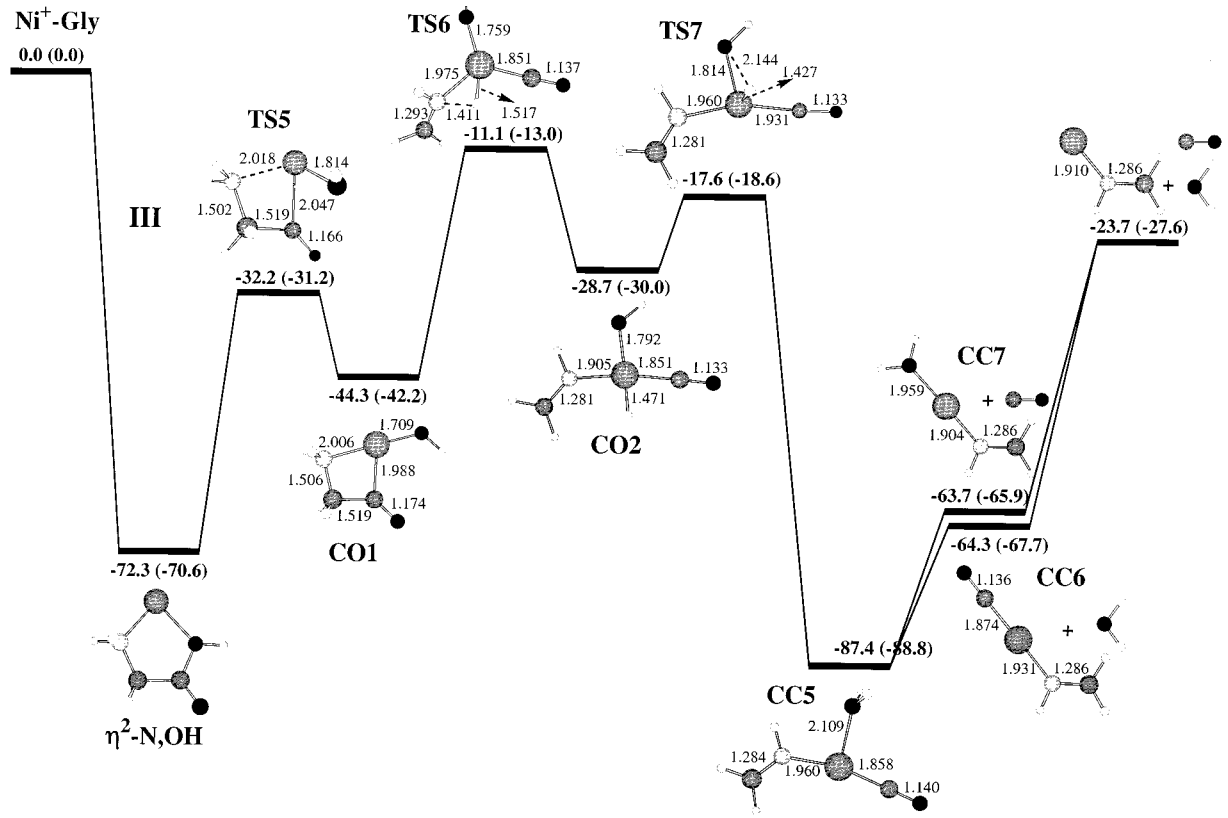

Figure 5. Schematic representation of the potential energy surface associated with the unimolecular reactions of [Ni−glycine]$^+$ starting with the Ni^+ insertion in the C−OH bond of the η^2**-N,OH** structure. Relative energies are in kcal/mol. Energies computed at the B3LYP/Basis2 level are shown in parentheses.

Figure 4 that in the **CC3** isomer the C−OH bond has been broken and both moieties, CO and OH, are now directly attached to the metal atom. The transfer of the hydrogen atom becomes now more easy and takes place through the transition state **TS4** with a barrier of 6.1 kcal/mol, leading to the isomer **CC5**. This complex is the global minimum of the potential energy surface being 87.4 kcal/mol below the reactants. In this isomer, Ni^+ is tricoordinated to H_2O, CO and CH_2NH and, therefore, a reductive elimination can produce either the loss of H_2O or the loss of CO leading to the products **CC6** + H_2O and **CC7** + CO, respectively. These dissociations are energetically favorable by 64.3 and 63.7 kcal/mol, respectively, with respect to the reactants.

As a summary of this mechanism, some features have to be pointed out. First of all, it can be observed in Figure 4 that all of the studied fragmentations are exothermic. However, the dissociation of the initial adduct to produce Ni^+-CHNH_2 + HCOOH (reaction path **I**) implies a very high energy barrier with a transition state being only 1.4 kcal/mol below the reactants. Moreover, this dissociation limit is less exothermic than the formation of **CC6** or **CC7** by more then 20 kcal/mol. These facts explain the small abundance of Ni^+-CHNH_2 detected in the experiments compared to the loss of water product.

Pathway **II** is much more favorable energetically and leads to the formation of the most exothermic products, namely **CC6** + H_2O and **CC7** + CO. However, the energy gap between both dissociation limits does not explain by itself the difference of the intensities between the corresponding peaks observed in the MIKE spectrum. This difference can also be due to other reasons. It can be observed in Figure 4 that the reorganization in the isomer **CC5** after the loss of H_2O to yield **CC7** must be much easier than the reorganization needed to yield **CC7**. On the other hand, other mechanisms can contribute to the loss of H_2O as will be discussed later.

C−O Insertion Mechanism. Figure 5 shows the computed mechanism (reaction path **III**) obtained when the Ni^+ metal cation inserts into the C−OH bond of the η^2**-N,OH** structure. It must be taken into account that this structure lies 12.4 kcal/mol above the most stable η^2**-N,O(1)** one. The insertion of the metal cation produces the **CO1** complex through an energy barrier of 40.1 kcal/mol. The **CO1** species is 44.3 kcal/mol more stable than the reactants and the Ni atom forms a four member ring with the nitrogen atom and the two carbon atoms. One of the hydrogen atoms of the NH_2 group of **CO1** is then transferred to the metal cation to lead to a tetracoordinated complex noted **CO2**. The transition state connecting both minima is **TS6** which is 11.1 kcal/mol below the reactants. A 1,2-hydrogen transfer connects minima **CO2** and **CC5**, the same complex found in reaction path **II**. The transition state **TS7** that connects these two minima with an energy barrier of 11.1 kcal/mol, is 17.6 kcal/mol below the reactants. Thus, this reaction path is also thermodynamically accessible and leads to the same products than reaction path **II**, **CC6** + H_2O and **CC7** + CO. However, reaction path **III** is considerably less favorable due to its high energy barrier.

Noninsertion Mechanisms. Finally, we have explored the mechanisms involving a 1,4-hydrogen transfer in the η^1**-N(2)** and η^1**-O(3)** structures (reaction paths **IV** and **V**, respectively). These mechanisms are shown in Figure 6. All attempts to locate a complex with the hydrogen atom transferred to the hydroxyl oxygen have failed because in all cases the H_2O molecule dissociates yielding **NI1** + H_2O in the case of η^1**-N(2)** and **NI2** + H_2O in the case of η^1**-O(3)**. It can be observed in Figure 6 that **NI2** is somewhat more stable than **NI1** and thus, **NI1** will probably evolve to **NI2** leading both mechanisms to the same

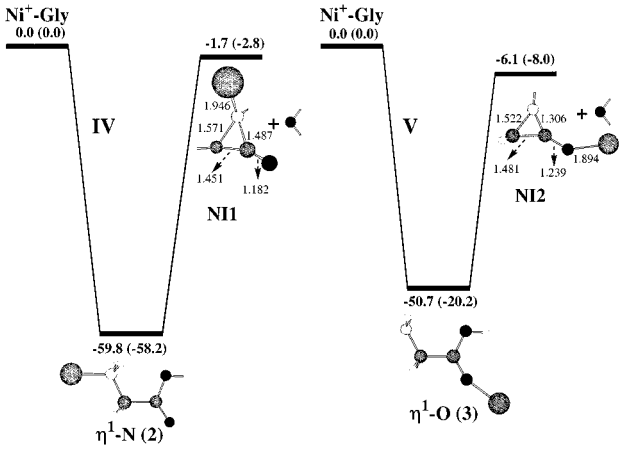

Figure 6. Schematic representation of the potential energy surface associated with the unimolecular reactions of [Ni−glycine]$^+$ starting from the η^1**-N(2)** and η^1**-O(3)** adducts. Relative energies are in kcal/mol. Energies computed at the B3LYP/Basis2 level are shown in parentheses.

final products. These reaction paths lead to the elimination of H_2O without energy barrier in excess and therefore contribute to the formation of the main product observed experimentally.

As found previously for the relative energies of the different isomers of [Ni−glycine]$^+$, the increase of the basis set does not produce significant changes in the barriers and reaction energies of the studied pathways.

Conclusions

Reactions between glycine and Ni^+ in the gas phase under FAB conditions produce the [Ni−glycine]$^+$ adduct. The structure of this adduct has been investigated by means of the B3LYP theoretical approach. Several coordination modes of Ni^+ to glycine have been considered. The ground-state structure has found to be a bidentate η^2**-N,O** one with the Ni^+ cation interacting with the nitrogen atom and the carbonyl oxygen. The relative energies of the different conformers can be explained in terms of the electrostatic and polarization energies and the relative stability of the glycine conformer involved in the complex with respect to the most stable structure of glycine.

The unimolecular reactivity of the [Ni−glycine]$^+$ ion has also been studied both experimentally and theoretically. The MIKE spectrum shows that the major fragmentation of the adduct corresponds to the loss of water. Other remarkable losses are observed to a minor extent, namely that of CO and CH_2O_2. The theoretical results show that all of these fragmentations are exothermic, with the loss of H_2O the most favorable one. The loss of CO is only about 2 kcal/mol less favorable, and the loss of CH_2O_2 or H_2O + CO is much higher in energy. Several reactive pathways can lead to these fragmentations. The pathway showing the lower activation barriers (**II**) corresponds to a insertion of the metal cation into the C−C bond of the most stable η^2**-N,O (1)** structure. This path leads to the formation of the very stable tricoordinated [(CH_2═NH)−Ni^+−(CO)(H_2O)] complex, which can be a precursor for the loss of H_2O and/or CO, and in both cases dissociation takes place without barrier in excess. The insertion of Ni^+ into the CO bond of the η^2**-N,-OH** structure (pathway **III**) leads to the same tricoordinated complex, but in this case the activation energy is more important.

The energy gap between loss of H_2O and loss of CO (2 kcal/mol) dos not entirely explain the differences between the intensities of the corresponding peaks observed in the spectrum. These differences can be due to the fact that other paths contribute to the loss of water, for example noninsertion mechanism such as **IV** and **V**. Although these two pathways are less favorable energetically than **II** or **III**, they take place in only one step. Thus, if we would introduce dynamical aspects, which are not taken into account in this study, these mechanisms could contribute significantly to the loss of water peak.

Acknowledgment. The use of computational facilities at the Institut de Developpement et de Recherche Scientifique (IDIRS) is gratefully acknowledged. L.R. acknowledges a postdoctoral Marie Curie grant from the UE.

References and Notes

(1) Eller, K.; Schwarz, H. *Chem. Rev.* **1991**, *91*, 1121.
(2) *Gas-Phase Metal Reactions*; Fontijn A., Ed.; North-Holland: Amsterdam, 1992.
(3) *Organometallic Ion Chemistry*; Freiser, B. S., Ed; Kluwer Academic Publishers: Dordrecht, 1995.
(4) McLafferty, F. W.; Schuddenmage, H. D. R. *J. Am. Chem. Soc.* **1969**, *62*, 1866.
(5) Cooks, R. G. *Collision Spectroscopy*; Plenum Press: New York, 1978.
(6) Senko, M. W.; Speir, J. P.; McLafferty, F. W. *Anal. Chem.* **1994**, *66*, 1866.
(7) Fraùsto da Silva, J. J. R.; Williams, R. J. P.; *The Inorganic Chemistry of Life*; Clarendon Press: Oxford, 1991.
(8) Tortajada, J.; Leon, E.; Morizur, J. P.; Luna, A.; Mo, O.; Yañez, M. *J. Phys. Chem.* **1995**, *99*, 9, 13890.
(9) Luna, A.; Amekraz, B.; Morizur, J. P.; Tortajada, J.; Mo, O.; Yañez, M. *J. Phys. Chem.* **1997**, *101*, 5931.
(10) Luna, A.; Amekraz, B.; Tortajada, J.; Morizur, J. P.; Alcamí, M.; Mo, O.; Yañez, M. *J. Am. Chem. Soc.* **1998**, *120*, 5411.
(11) Cerda, B. A.; Wesdemiotis, C. *J. Am. Chem. Soc*. **1995**, *117*, 9734.
(12) Polce, M. J.; Beranova, S.; Nold, M. J.; Wesdemiotis, C. *J. Mass Spectrom.* **1996**, *31*, 1073.
(13) Wen, D.; Yalcin, T.; Harrison, A. G. *Rapid Commun. Mass Spectrom.* **1995**, *9*, 1155.
(14) Yalcin, T.; Wang, J.; Wen, D.; Harrison, A. G. *J. Am. Soc. Mass Spectrom.* **1997**, *8*, 749.
(15) Bouchonnet, S.; Hoppiliard, Y.; Ohanessian, G. *J. Mass Spectrom.* **1995**, *30*, 172.
(16) Lavanant, H.; Hoppiliard, Y. *J. Mass Spectrom.* **1997**, *32*, 1037.
(17) Lavanant, H.; Hecquet, E.; Hoppiliard, Y. *Int. J. Mass Spectrom.* **1999**, *185*, 11.
(18) Rogalewicz, F.; Hoppiliard, Y.; Ohanessian, G. *Int. J. Mass Spectrom.* **2000**, *201*, 307.
(19) Lei, Q. P.; Amster, I. J. *J. Am. Soc. Mass Spectrom.* **1996**, *7*, 722.
(20) Hoyau, S.; Ohanessian, G. *Chem. Eur. J.* **1998**, *4*, 1561.
(21) Hoyau, S.; Ohanessian, *J. Am. Chem. Soc.* **1997**, *119*, 2016.
(22) Bertran, J.; Rodriguez-Santiago, L.; Sodupe, M. *J. Phys. Chem. B* **1999**, *103*, 2310.
(23) Marino, T.; Russo, N; Toscan, N. *J. Inorg. Biochem.* **2000**, *79*, 179.
(24) Harrison, A. G.; Mercer, R. S.; Reinee, E. J.; Young, A. B.; Boyd, R. K.; March, R. E.; Porter, C. J. *Int. J. Mass Spectrom. Ion Process*. **1986**, 74, 13.
(25) (a) Becke, A. D. J. Chem. Phys. **1993**, 98, 5648. (b) Lee, C.; Yang, W.; Parr, R. G. *Phys. Rev. B* **1988**, 37, 785. (c) Stevens, P. J.; Devlin, F. J.; Chablowski, C. F.; Frisch, M. J. *J. Phys. Chem.* **1994**, 98, 11623.
(26) Holthausen, M. C.; Heineman, C.; Cornehl, H. H.; Koch, W.; Schwarz, H. *J. Chem. Phys*. **1995**, *102*, 4931.
(27) Adamo, C.; Lelj, F. *J. Chem. Phys*. **1995**, *103*, 10605.
(28) Blomberg, M. R. A.; Siegbahn, P. E. M.; Svensson, M. *J. Chem. Phys*. **1996**, *104*, 9546.
(29) Rodríguez-Santiago, L.; Sodupe, M.; Branchadell, V. *J. Chem. Phys.* **1996**, *105*, 9966.
(30) Bauschlicher, C. W.; Ricca, A.; Partridge, H.; Langhoff, S. R. in *Recent Advances in Density Functional Theory*, Part II. Chong, D. P. Ed.; World Scientific Publishing Company: Singapore, 1997.
(31) Luna, A.; Amekraz, B.; Tortajada, J. *Chem. Phys. Lett.* **1997**, *266*, 31.
(32) Luna, A.; Alcamí, M.; Mo, O.; Yañez, M. *Chem. Phys. Lett.* **2000**, *320*, 129.
(33) Pulkkinen, S; Noguera, M.; Rodríguez-Santiago, L.; Sodupe, M.; Bertran, J. *Chem. Eur. J*. **2000**, *6*, 4393.
(34) Lelj, F.; Adamo, C.; Barone, V. *Chem. Phys. Lett.* **1994**, *230*, 189.
(35) Barone, V.; Adamo, C.; Lelj, F. J.*Chem. Phys.* **1995**, *102*, 364.

(36) Stepanian, S. G.; Reva, I. D.; Radchenko, E. D.; Rosado, M. T. S.; Duarte, M. L. T. S.; Fausto, R.; Adamowicz, L. *J. Phys. Chem. A* **1998**, *102*, 1041.

(37) Stepanian, S. G.; Reva, I. D.; Radchenko, E. D.; Adamowicz, L. *J. Phys. Chem. A* **1998**, *102*, 4623.

(38) Wachters, A. J. H. *J. Chem. Phys*. **1970**, *52*, 1033.

(39) Hay, P. J. *J. Chem. Phys.* **1977**, *66*, 4377.

(40) Dunning, T. H. *J. Chem. Phys.* **1970**, *53*, 2823.

(41) Gaussian 98, Revision A.7, Frisch, M. J.; Trucks, G. W.; Schlegel, H. B.; Scuseria, G. E.; Robb, M. A.; Cheeseman, J. R.; Zakrzewski, V. G.; Montgomery, Jr., J. A.; Stratmann, R. E.; Burant, J. C.; Dapprich, S.; Millam, J. M.; Daniels, A. D.; Kudin, K. N.; Strain, M. C.; Farkas, O.; Tomasi, J.; Barone, V.; Cossi, M.; Cammi, R.; Mennucci, B.; Pomelli, C.; Adamo, C.; Clifford, S.; Ochterski, J.; Petersson, G. A.; Ayala, P. Y.; Cui, Q.; Morokuma, K.; Malick, D. K.; Rabuck, A. D.; Raghavachari, K.; Foresman, J. B.; Cioslowski, J.; Ortiz, J. V.; Baboul, A. G.; Stefanov, B. B.; Liu, G.; Liashenko, A.; Piskorz, P.; Komaromi, I.; Gomperts, R.; Martin, R. L.; Fox, D. J.; Keith, T.; Al-Laham, M. A.; Peng, C. Y.; Nanayakkara, A.; Gonzalez, C.; Challacombe, M.; Gill, P. M. W.; Johnson, B.; Chen, W.; Wong, M. W.; Andres, J. L.; Gonzalez, C.; Head-Gordon, M.; Replogle, E. S.; Pople, J. A. Gaussian, Inc.: Pittsburgh, PA, 1998.

(42) Bauschlicher, C. W., Jr.; Langhoff, S. R.; Barnes, L. A. *J. Chem. Phys.* **1989**, *91*, 2399.

(43) Krishnan, R.; Binkley, J. S., Seeger, R.; Pople, J. A. *J. Chem. Phys.* **1980**, *72*, 650.

(44) (a) Weinhold, F.; Carpenter, J. E. *The structure of small molecules and ions*; Plenum: New York, 1988. (b) Reed, A. E.; Curtiss, L. A.; Weinhold, F. *Chem. Rev.* **1988**, *88*, 899.

(45) Dean, L. K. L.; Busch, K. L. *Org. Mass Spectrom*. **1988**, *24*, 733.